Sustainable Energy & Fuels

ROYAL SOCIETY OF CHEMISTRY

PAPER

View Article Online
View Journal | View Issue



Cite this: *Sustainable Energy Fuels*, 2025, **9**, 2389

# Push–pull amino-substituted heteroleptic iron N-heterocyclic carbene photosensitizers in dye-sensitized solar cells: optimization and characteristics†

Samuel Persson, [a] Iacopo Benesperi, [bc] Yogesh Goriya, [a] Dnyaneshwar Kand, [a] Suresh Rayavarapu, [a] Timo Keller, [b] Marina Freitag *[b] and Kenneth Wärnmark *[a]

In this work, four dyes—consisting of heteroleptic iron N-heterocyclic carbene (NHC) complexes—were investigated in dye-sensitized solar cell (DSC) applications to explore their behavior and interactions with the overall cell. Three of the four dyes contained amino-based electron donor moieties, while one was without this type of structure, and instead had only a hydrogen atom. Compared to earlier investigations, the characteristics of the DSC devices were improved by the use of a UV-curing glue to seal the cells, by lowering the concentration of sensitization baths, and by altering the composition of the $TiO_2$ substrates. This resulted in devices with power conversion efficiencies of up to 1.3%. Optimizations previously made to the electrolyte for DSCs incorporating iron–NHC devices were however found to be detrimental for amino-substituted complexes, giving worse results for all measured characteristics of these dyes. There was furthermore a significant hysteresis effect for devices made from each dye, hitherto not reported for iron–NHC complexes as dyes, where the scan direction strongly influenced the open circuit voltage and thereby also the efficiency.

Received 19th December 2024
Accepted 13th March 2025

DOI: 10.1039/d4se01772b

rsc.li/sustainable-energy



## Introduction

The use of solar cells is one of the most promising approaches for generation of electrical power in the future, due to the large amount of solar irradiation reaching the planet.[1] Dye-sensitized solar cells (DSCs) have, since their introduction in their modern form by O'Regan and Grätzel in 1991,[2] offered an intriguing route for solar harvesting due to their particular properties, such as low cost and simple manufacturing, flexibility and transparency, and low toxicity.[3–5] An integral component of any DSC is the molecular photosensitizer, commonly called the dye, responsible for uptake of light *via* its own photoexcitation. Dyes used in DSCs have classically been made from rare metals, such as ruthenium.[4] To enable the wider usage of DSCs, there is a need to move away from such scarce metals as the basis for the dye, and towards earth-abundant metals and organic structures.[6,7]

The use of N-heterocyclic carbene (NHC) complexes with iron has received some attention as a promising strategy to make this metal into a competent photosensitizer.[8–11] The use of these iron–NHC photosensitizers as dyes in DSCs has also been investigated over the last decade, in parallel with the overall development of this type of photosensitizers.[12–14] While initial results in 2015 showed only a negligible PCE of 0.13%,[15] studies suggesting close to unitary injection of photoexcited electrons[16] maintained interest in these dyes and there has since been a steady improvement of this concept. Improvements on dye design for iron–NHC complexes in DSCs have been mainly focused on the introduction and modification of peripheral ligand moieties to tune the properties of the dye. It has generally been found that the use of heteroleptic systems with one anchoring ligand and an opposite ligand lacking any electron withdrawing group has been the most successful.[17–19] Apart from dye design, efficiency has further been significantly improved by optimizing the composition of the electrolyte.[17,20–22] However, the use of the redox mediator $Co(bpy)_3$ (employed with great success in many modern DSC-systems), intended to replace the common but corrosive $I^-/I_3^-$ redox couple, was found to not be beneficial in conjunction with iron–NHC dyes.[19]

The most successful dyes based on iron–NHCs to date use linearly aligned push–pull structures, together with a highly

[a]*Centre for Analysis and Synthesis, Department of Chemistry, Lund University, Box 124, SE-22100 Lund, Sweden. E-mail: kenneth.warnmark@chem.lu.se*

[b]*School of Natural and Environmental Science, Newcastle University, Bedson Building, NE1 7RU, Newcastle upon Tyne, UK. E-mail: marina.freitag@newcastle.ac.uk*

[c]*Department of Chemistry, NIS Interdepartmental Centre and INSTM Reference Centre, University of Turin, Via Quarello 15/A, 10135 Torino (TO), Italy*

† Electronic supplementary information (ESI) available: Further details and experimental section. See DOI: https://doi.org/10.1039/d4se01772b

tuned acetonitrile (ACN)-based electrolyte solution containing the $I^-/I_3^-$ redox mediator and several salts as additives to improve efficiency. This has led to reported efficiencies by Gros and coworkers in 2021 as high as 1.8%, for DSC devices sensitized with a single iron–NHC complex. It was however suggested that this success, at least partly, stemmed from an improvement in the absorptivity of the dye, rather than a proper realization of a push–pull design to improve the dynamics of electron injection and prevention of charge recombination.[18] Additionally, PCEs as high as 2.1% have been reached in 2023, also by Gros and coworkers, by co-sensitization of two different homoleptic iron–NHC complexes, again by achieving better coverage of the solar spectrum.[23]

Here, we present a study using a series of heteroleptic iron–NHC complexes previously known in the literature,[18,19,24] in order to gain a better understanding of how these dyes function in DSC devices and improve their efficiency. The examined dyes were [Fe(cpbmi)(pbmi)]$(PF_6)_2$ (**1**), [Fe(cpbmi)(dtapbmi)]$(PF_6)_2$ (**2**), [Fe(cpbmi)(daapbmi)]$(PF_6)_2$ (**3**), and [Fe(cpbmi)(dmapbmi)]$(PF_6)_2$ (**4**) (Fig. 1; cpbmi = 1,1′-(4-carboxypyridine-2,6-diyl) bis(3-methylimidazole-2-ylidene); pbmi = 1,1′-(pyridine-2,6-diyl) bis(3-methylimidazole-2-ylidene); dtapbmi = 1,1′-(4-(di(*p*-tolyl)amino)pyridine-2,6-diyl) bis(3-methylimidazole-2-ylidene); daapbmi = 1,1′-(4-(di(*p*-anisyl)amino)pyridine-2,6-diyl) bis(3-methylimidazole-2-ylidene); dmapbmi = 1,1′-(4-(*N*, *N*-dimethylamino)pyridine-2,6-diyl) bis(3-methylimidazole-2-ylidene)). With these complexes as a basis for the study of heteroleptic iron–NHC dyes, we investigated novel approaches to the assembly of DSC devices using these types of complexes and studied the characteristics and properties of the resulting devices.

## Results and discussion

### Synthesis

The complexes utilized in this study were generally synthesized according to the same principles as previously reported for similar substances. The procedure, introduced for iron–NHC complexes by Gros and coworkers,[24] involves the mixing of both ligands to be introduced to the complex, and then performing the complexation by deprotonation of the pre-carbene ligand, followed by addition of $FeBr_2$ (Scheme 1). The reaction sequence led to a mixture of complexes that could then be separated by chromatography.

Within this work there are a number of modifications to previously published procedures for the purification of complexes **1** and **4**, such as stationary phase used for chromatography, as these modifications were found to be more functional in our hands. In addition, for the synthesis of complex **4**, the dimethylamino-derived ligand seemingly outcompeted the carboxylic acid-containing ligand for the attachment to iron(II) ions, giving a detrimental excess of the homoleptic iron(II) complex with two NHC ligands containing the dimethylamino moiety. This issue was circumvented by the addition of two equivalents of $FeBr_2$, giving the desired heteroleptic complex in a reasonable yield (Scheme 1). See ESI† for detailed experimental procedures (Fig. S1–S8 in ESI† for NMR spectra of complexes synthesized by new procedures).

### Steady state absorption

Iron–NHC complexes bearing carboxylic acid-substituted ligands have a strong propensity to deprotonate at low concentration in acetonitrile, and this can have significant effects on absorption spectra.[19,25] To counter this issue, care was taken to keep the complexes protonated during measurement. A constant protonation ratio of the dyes was accomplished by the addition of methanesulfonic acid to the acetonitrile solvent, as demonstrated before.[19]

Steady state absorption spectra of dyes **1** and **4** were recorded, as these spectra had not been previously obtained under these conditions. Extinction coefficients for complexes **2** and **3** were taken from literature (Fig. 2).[19]

Spectral shape and extinction coefficient ($\varepsilon$) for [Fe(cpbmi)(dmapbmi)]$(PF_6)_2$ (**4**) were in line with previous findings,[18] although the $\varepsilon$ was here found to be slightly higher. Full spectrum and $\varepsilon$ of [Fe(cpbmi)(pbmi)]$(PF_6)_2$ (**1**) in solution were not previously found in the literature, but findings here were consistent with reported data for this complex.[17]

### Photovoltaic studies

All devices fabricated in this study utilized the $I^-/I_3^-$ redox couple, as well as 1-methyl-3-propylimidazolium iodide (MPII)

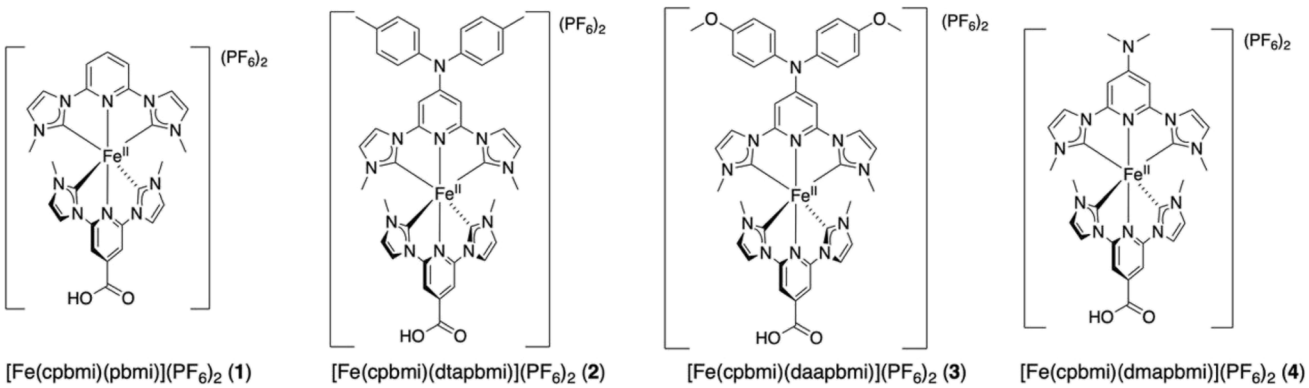


Fig. 1 Structure of the four iron–NHC dyes used in this study.

 

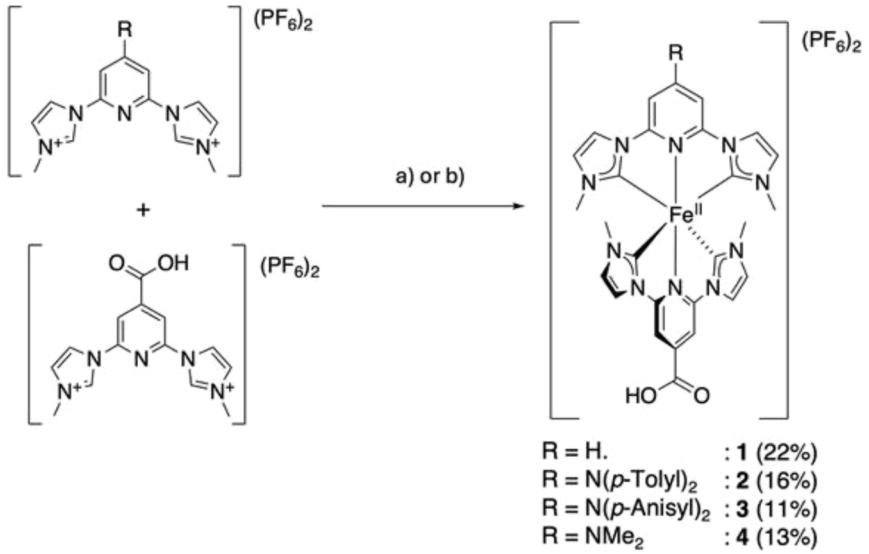


Scheme 1 Procedure to form Fe–NHC dyes used in this study. (a) 1. KO*t*-Bu (THF, 3 eq.), 0 °C, DMF, 2. $FeBr_2$ (1 eq.), DMF, rt (used for **1–3**). (b) 1. KO*t*-Bu (THF, 3 eq.), −78 °C, THF, 2. $FeBr_2$ (2 eq.), THF, rt (used for **4**).

as an additive to the electrolyte solution (in majority with 3-methoxypropionitrile (MPN) as the solvent). Additionally, the various dyes were co-adsorbed with chenodeoxycholic acid in sequential dye baths, as this is known to improve the efficiency of this type of dyes.[19]

Several optimizations were made to the components and assembly of solar cells. For instance, device assembly with UV-curing glue instead of thermoplastic surlyn, the latter used in previous reports of these dyes,[17–19] led to a significant improvement in efficiency by greatly increasing $J_{SC}$ (in certain cases more than doubling the current), with a smaller loss in $V_{OC}$ (<0.03 V for all investigated cases; Table S1 in ESI†). This improved efficiency was unexpected, as the direct contact of the Pt-based counter-electrode with the $TiO_2$-based photoelectrode was believed to lead to short circuiting of the device. This was however not the case here, and assumedly the dense scattering

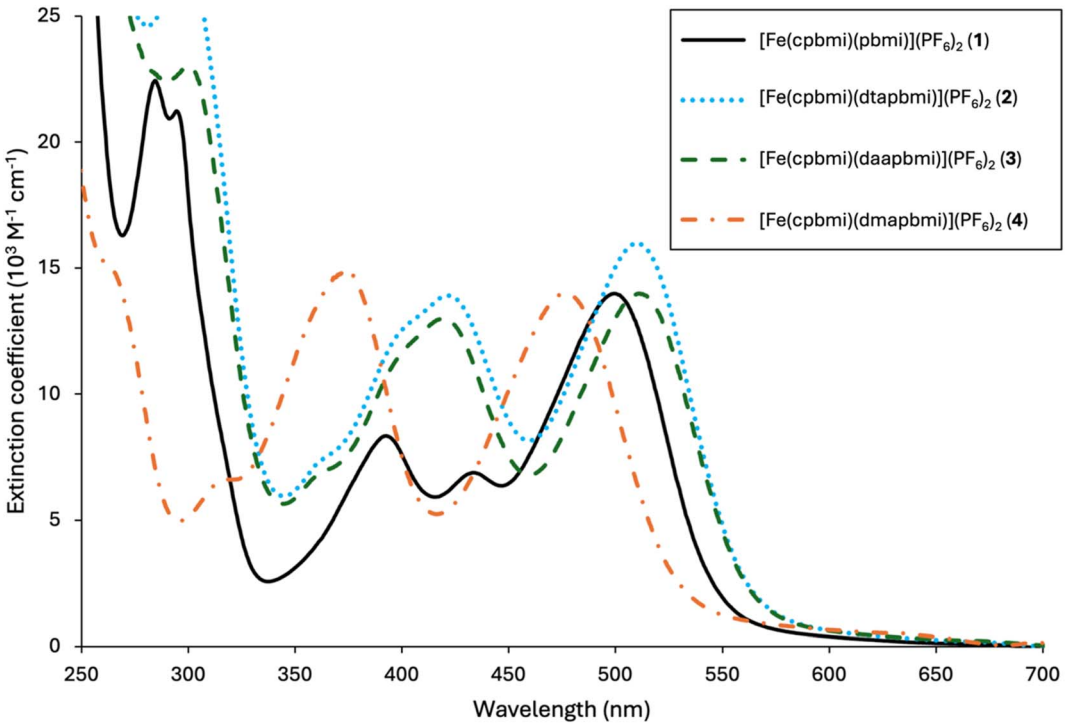


Fig. 2 Steady state absorption spectra of dyes **1–4**, all dissolved in a solution of 0.1 M tetrabutylammonium methanesulfonate and 0.1 M methanesulfonic acid in acetonitrile.

layer serves to isolate the electrodes from one another to a sufficient degree for the correct functioning of the devices. The improvement in $J_{SC}$ of the devices can be linked to the reduction of the diffusion distance necessary for the redox mediator in the electrolyte to carry the charge for dye regeneration.

Compared to earlier publications regarding these dyes,[17–19] sensitization using dye baths with a lower dye concentration (0.05 mM) was found to be beneficial for dyes **2–4**. This improvement occurs despite lower dye loading, clearly visible by simple observation of the coloration of the substrates after sensitization. Previous studies with 0.2 mM dye baths of dyes **2** and **3** resulted in dye loadings of $9.87 \times 10^{-5}$ and $6.55 \times 10^{-5}$ mmol cm$^{-2}$, respectively.[19] The use of 0.05 mM sensitization baths in the present work leads to lower dye loadings that nonetheless yield improved photovoltaic performance due to reduced aggregation. For a higher dye loading to negatively affect the efficiency of the cell, aggregation between dye molecules on the titania surface is probable; either between those molecules adsorbed to the surface, or through non-covalent interactions between adsorbed dyes and dyes which are not adsorbed. Either interaction leads to detrimental effects by quenching excited states, resulting in photoexcitation that does not lead to electron injection into the semiconductor. On the contrary, dye **1** showed the greatest efficiency using the dye bath of previously reported concentration (0.2 mM; Table S2 in ESI†).[17] These findings suggest that aggregation is caused by the introduction of amine substituents, as seen in dyes **2–4**. The *N*-aryl groups introduced for dyes **2** and **3** can reasonably induce aggregation due to π–π interactions. This is also in line with the improvement of efficiency found using lower concentration of sensitization baths being most pronounced for dyes **2** and **3**. However, since the benefit of lower dye loading is also present for dimethylamine-substituted dye **4**, another effect must also be at play, such as hydrogen-bonding interactions, plausibly between the aryl amines and carboxylic acid. The optimizations of sealant and sensitization combined gave devices with PCE values of 1.0–1.2%. As a matter of fact, we have previously shown by UV/vis dilution experiments involving the free complexes **2**, **3**, and the reference complex $[Fe(cpbmi)_2](PF_6)_2$ (cpbmi = 1,1′-(4-carboxypyridine-2,6-diyl)bis(3-methylimidazole-2-ylidene)), the latter containing no *N*-aryl amino groups, that there is a large change in both the wavelength of the absorption maximum and shape of the absorption spectra upon dilution, much more severe for compounds **2** and **3**, compared to the reference complex upon dilution.[19] This could, in addition to change in protonation state,[19] also indicate aggregation, being worse for the dyes containing the *N*-aryl amino groups.

The PCE of the various devices was highest with MPN-based electrolyte solutions (rather than ACN) of $I^-/I_3^-$ (with $Li^+$ as the cations) with the addition of an imidazolium-based ionic liquid, in accordance with previous findings by Karpacheva *et al.*[20] We investigated the effect of the addition of further additives to the electrolyte as introduced by Gros and coworkers, namely the use of $MgI_2$, guanidinium thiocyanate (GuSCN), tetrabutylammonium iodide (TBAI) and 1-methyl-3-propylimidazolium iodide (MPII).[17,18] The use of these additives was investigated in both ACN- and MPN-based electrolyte solutions. The salts were poorly soluble in the less polar MPN solvent, and a saturated solution of the additives was thus used in this case. For three of the four dyes (**2–4**) in this study, it was found that the saturated solution in MPN gave better results with regards to all measured parameters compared to the ACN-based solution with fully dissolved additives (with a relative decrease in PCE between 41%-19% for the ACN solution). For these dyes, the extra additives in MPN showed little effect compared to the simpler electrolyte solution mentioned above, the former giving <0.1% lower PCE for the amino-substituted dyes investigated. Efficiency was improved for dye **1**, with a relative PCE increase of 17% when using an ACN-based electrolyte solution with the aforementioned additional additives (Tables S3 and S4 in ESI†). As the negative effect from the additives was present only for the dyes containing amino moieties, the detrimental interaction should reasonably be linked to these substituents. The most likely explanation is a coordination between the amino group of the dye and the added cations of high charge density. This coordination would negatively impact the directionality of the dyes, as it introduces positive charges on the side of the dye opposite to the $TiO_2$, pulling electrons away from the injection site. The smaller number of ions present in MPN, due to lower solubility, more or less removed this effect. In the case of dye **1**, the lack of a substituent on the ligand exposed to the electrolyte removed the possibility for coordinating cations in such a way, instead giving improvements in line with previous reports.[17] It then follows that this detrimental effect for dyes **2–4** may also be present to some degree with the lithium ions contained in all electrolytes, hampering the efficacy of dyes with amine-based electron donating groups. For the purpose of a simpler system to study and making a one-to-one comparison between each dye, we decided to proceed by using the simpler $I^-/I_3^-$-redox mediator, with MPII as the only additive (Fig. S9 and Table S5 in ESI†).

We finally investigated the use of $TiO_2$ substrates made from a 1 : 1 mixture of 18 nm and 30 nm particles, as opposed to the simpler $TiO_2$ substrates fabricated with 18 nm particles alone used for the studies discussed above. Devices made from these substrates showed an improvement in PCE of varying magnitude for all investigated dyes. These improvements were linked to an increase in $J_{SC}$, and thus to improved light absorption by the photoanode. The largest improvement in PCE was observed for dye **1**, giving a relative improvement of 8% (for the average device; 20% for the best performing devices); dye **2** and **3** showed relative improvements of around 4%, while dye **4** showed close to no improvement (Table 1 and Fig. 3). These results could be related to the different $TiO_2$ pore structure obtained using a mixture of particle sizes, allowing for greater dye loading. In the fully optimized cells, a clear but small (about 20 mV, less than 5%) trend of improved $V_{OC}$ can be seen for the dyes substituted with amine donors. The largest improvement in $V_{OC}$ was observed with dye **4**, which has the most electron donating substituent. This may point to the fact that a stronger electron donation from the substituent on the dye leads to a somewhat larger buildup of charge separation in the surface,

 

Table 1 Solar cell characteristics for best performing cells (with regards to PCE) sensitized with dyes **1–4**, on 18 nm and 30 nm particle $TiO_2$, scanning from short circuit to open circuit. Open-circuit voltage ($V_{OC}$), short-circuit current density ($J_{SC}$), fill-factor (FF) and power conversion efficiency (PCE). Average of six cells from the same batch, with standard deviations, within parentheses

| Dye | $V_{OC}$ (mV) | $J_{SC}$ (mA cm$^{-2}$) | $J_{SC,IPCE}$ (mA cm$^{-2}$) | FF | PCE (%) |
|---|---|---|---|---|---|
| [Fe(cpbmi)(pbmi)]$(PF_6)_2$ (**1**) | 438 (439 ± 1) | 4.93 (4.2 ± 0.3) | 5.11 | 0.584 (0.591 ± 0.002) | 1.26 (1.10 ± 0.05) |
| [Fe(cpbmi)(dtapbmi)]$(PF_6)_2$ (**2**) | 447 (454 ± 1) | 4.41 (4.08 ± 0.06) | 4.49 | 0.597 (0.599 ± 0.003) | 1.18 (1.108 ± 0.009) |
| [Fe(cpbmi)(daapbmi)]$(PF_6)_2$ (**3**) | 459 (458 ± 3) | 3.71 (3.4 ± 0.2) | 3.85 | 0.596 (0.613 ± 0.005) | 1.02 (0.94 ± 0.03) |
| [Fe(cpbmi)(dmapbmi)]$(PF_6)_2$ (**4**) | 459 (471 ± 2) | 4.46 (4.21 ± 0.08) | 4.54 | 0.614 (0.613 ± 0.0004) | 1.26 (1.211 ± 0.006) |

as the groups introduced supposedly hamper charge recombination due to the electron donating effects of the amino substituents. An alternative explanation could however be a matter of different redox potential of the dyes and therefore different driving force for dye regeneration with the $I^-/I_3^-$-electrolyte. Simultaneously, the dyes bearing aryl-substituted amine donors yield lower $J_{SC}$, plausibly due to lower dye-loading due to larger steric bulk (giving dye **3**, with largest substituents, the lowest $J_{SC}$).

Incident photon-to-current conversion efficiency (IPCE) measurements gave spectra of the same shape for all four dyes, independent of $TiO_2$ substrate. The only difference observed between the different dyes and substrates was in the magnitude of the IPCE values. IPCE did not agree fully with the $J_{SC}$ measurements, with all complexes showing somewhat higher $J_{SC}$ when calculated from the IPCE measurements (Table 1). The wavelength giving the strongest peak in the IPCE spectra was otherwise consistent with the wavelength of the MLCT bands found in steady state absorption (Fig. 2) for all dyes,[19] with a modified intensity attributable to dye loading. The IPCE spectra were red-shifted to varying degrees compared to the steady state absorption, which could stem from the slight change in electronic structure upon binding the electron accepting ligand to the $TiO_2$ layer (Fig. S10 in ESI†).

The differences in electron recombination lifetimes were generally very small between the different dyes, when sensitized under the same conditions. The main difference observed was that devices made with 18 nm $TiO_2$ particles showed significantly longer lifetimes at higher charge densities, compared to those made from substrates with $TiO_2$ of mixed particle sizes (Fig. S11 in ESI†).

As dyes in this manuscript have been comprehensively characterized by fs-transient absorption (TA) spectroscopy in our previous studies, which showed efficient electron injection (with time constants as short as <100 fs–3 ps) and fast charge recombination dynamics,[16,19] we assert that additional TA measurements in the current study would be redundant. The new photovoltaic performance parameters reported here are entirely consistent with these previously determined kinetic characteristics and confirm that our dyes operate similar to their extensively studied analogues.

A further finding was that all devices manufactured within this study showed significant hysteresis during *J–V* scans. Scanning from open circuit (OC) to short circuit (SC) showed a significantly higher efficiency compared to scanning from SC

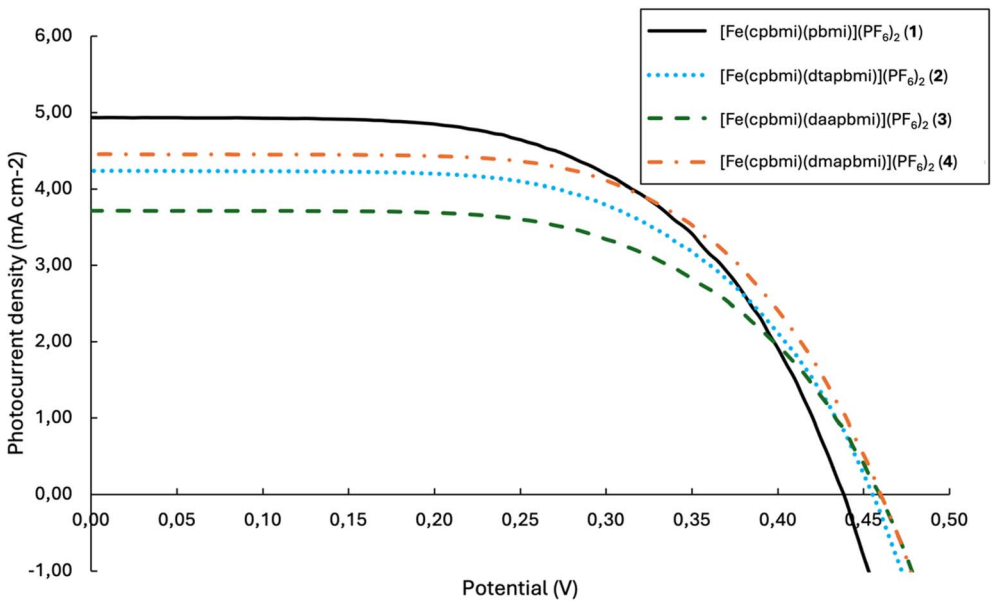


Fig. 3 Measured *J–V* characteristics at AM 1.5G illumination for best performing solar cells (with regards to PCE) sensitized with dyes **1–4**, on 18 nm and 30 nm particle $TiO_2$, scanning from short circuit to open circuit.

to OC. Generally, $J_{SC}$ was mostly unaffected by the shift in scan direction, while $V_{OC}$ was significantly increased for each investigated device when scanning from OC to SC. There were further varying degrees of distortion around the maximum power point (MPP) for all investigated dyes, when scanning from OC to SC (Fig. S12 and S13 in ESI†). These distortions led to an artificial improvement in fill factor (FF). Due to these distortions, we refrain from presenting the parameters taken from these scans as accurate (observed parameters may be found in Tables S6 and S7 in ESI†).

To further investigate these hysteresis effects, we measured cells sensitized with each dye under constant voltage, corresponding to the apparent $V_{MPP}$ (voltage at maximum power point) for each scan direction. These investigations gave PCE values of a magnitude that were intermediate between those observed in either scan direction. The PCE values were further found to drop over time during the measurement. This drop in PCE was more pronounced when measuring at a potential corresponding to a $V_{MPP}$ for the OC to SC scan (Fig. S14 in ESI†). We attribute the PCE decreasing over time to an instability of the devices under illumination. The reason the PCE decreases faster under conditions corresponding to $V_{MPP}$ of the OC to SC scan, would then be due to this being at a voltage higher than the actual MPP, where the impact of the instability is greater.

The hysteresis effect was smaller in devices using $TiO_2$ films with mixed particle sizes, but it was still present to some extent. This led to devices with substrates from only 18 nm particles to appear more efficient than those with mixed particle sizes, when scanning from OC to SC (with the exception of dye **1**, which was most efficient with the mixed particle substrates no matter the scan direction; Table S7 in ESI†).

Hysteresis effects in DSCs have previously been linked to capacitance between semiconductor and electrolyte in thicker layers of $TiO_2$.[26] Since an uncommonly thick $TiO_2$ was applied in the fabrication of the devices described herein (see ESI†), this effect could likely also be present here. A thicker $TiO_2$ layer has likewise been applied in previous studies of DSCs using Fe–NHC based dyes.[17–19,23] This is further corroborated by the smaller hysteresis effect found in devices with mixed $TiO_2$ particles, as the shorter electron lifetimes and lower charge densities in these devices points to a lower capacitance (Fig. S11 in ESI†). The hysteresis effect is largest for dye **1** and smaller for the three amino-substituted dyes **2–4** (Fig. S13, Tables S6 and S7 in ESI†). This could hint at the magnitude of the hysteresis effect being linked to the steric protection of the surface by the dyes. This is because the hysteresis effect can be linked to cations in the electrolyte having access to the semiconductor surface, in order to maintain the capacitance.[27] A clear relationship between steric encumbrance and magnitude of the hysteresis effect is not clearly noticeable at full sun illumination, but a clearer correlation can be seen at 10% sun illumination (Fig. S15 in ESI†). Measurements of the best performing cells at 10% consistently showed somewhat lower PCE values for all dyes, with an average relative decrease in PCE of about 22% when compared to full sunlight. Furthermore, the hysteresis effects present in measurements under full sunlight were significantly more pronounced under 10% sunlight, showing more than 120 mV higher $V_{OC}$ (an average increase in voltage of 43%) when scanning from OC to SC. The distortion around the MPP was likewise much more noticeable under 10% sunlight. In the most extreme case (that of devices sensitized by complex **1**), the distortion around the MPP was so significant that a current approximately twice as high as $J_{SC}$ was observed, when measuring from OC to SC. This distortion in turn led to an unreasonable FF of >1. The *J–V* measurements scanning from SC to OC again showed more reasonable data (Fig. S15 and Table S8 in ESI†). The more pronounced distortion at lower illumination can again be linked to the presence of capacitance within the solar cell. The smaller number of injected electrons (due to a smaller number of incoming photons) allows for a larger portion of these electrons to be maintained by capacitance, as less overall charge needs to be accumulated for a relatively larger effect to be observed.

The presence of the hysteresis effect makes comparison between these and other published results difficult, as scan direction is rarely noted in the literature. Known to us is that dyes **2** and **3** were previously measured with a scan direction from OC to SC. Under the same conditions we obtain here PCEs of 1.5% and 1.3%, for dye **2** and **3** respectively. Furthermore, scanning from OC to SC gave PCE values of up to 1.7% (found in dye **1**; 1.6% was achieved for dye **4**). These values outperform previously reported examples of all four dyes (1.4%, 1.3%, 0.9% and 1.2%, for dye **1**, **2**, **3**, and **4**, respectively).[17–19]

## Conclusion

Four dyes were investigated in DSC applications under various conditions. These dyes were all previously published, heteroleptic iron–NHC complexes, based on the parent structure of $[Fe(cpbmi)(pbmi)]^{2+}$ (**1**), with all except the parent complex having various tertiary amine substituents on the non-anchoring side of the complex. The efficiency of devices for all investigated dyes could be improved by various optimizations to the solar cell architecture. The use of UV-curing glue and a lower concentration of dye in sensitization baths provided the greatest improvement in efficiency, with a smaller improvement also being afforded using a $TiO_2$ paste of mixed particle sizes. The introduction of amine substituents introduced on the dyes led to improved $V_{OC}$, compared to the unsubstituted parent dye **1**, but larger *N*-aryl substituents gave lower $J_{SC}$.

Simultaneously, the implementation of an electrolyte solution with various additives ($MgI_2$, GuSCN, and TBAI), previously reported as beneficial for the use with iron–NHC based dyes, was found to be detrimental for the performance of the amino-substituted dyes, compared to a simpler MPN-based electrolyte solution consisting of a $I^-/I_3^-$ redox couple with MPII as the only additive. This suggests that care needs to be taken when optimizing the solar cells using dyes of the type described herein, as unwanted interactions may occur between certain ligand structures and excessive additives. Additives may thus need to be investigated on a dye-by-dye basis.

Furthermore, a significant hysteresis effect was found for all devices investigated, where the scan direction strongly influenced the $V_{OC}$ and thereby also the efficiency. This hysteresis

 

was also accompanied by a distortion of the *J–V* curve when scanning from OC to SC. These findings show that investigating DSCs using this family of dyes should be accompanied by consideration and reporting of the methods used for characterization. These findings may also prompt further investigation of this property, as the mechanism behind it has not been closely interrogated here.

## Conflicts of interest

There are no conflicts to declare.

## Acknowledgements

We thank the reviewers for their valuable comments. The Swedish Strategic Research Foundation (EM16-0067) and the Knut and Alice Wallenberg Foundation (2018.0074) are gratefully acknowledged for support. S. P. acknowledges support from the Erasmus+ programme. I. B. acknowledges the PNA4Energy project, funded under the MUR program "PNNR M4C2 Initiative 1.2: Young Researcher – Seal of Excellence" (CUP: D18H22001950007), and the support from Project CH4.0 under the MUR program "Dipartimenti di Eccellenza 2023–2027" (CUP: D13C22003520001). K. W. acknowledges support from the Swedish Research Council (VR 2020-03207), the Swedish Energy Agency (Energimyndigheten, P48747-1), the LMK Foundation, and the Sten K Johnson Foundation.

## References

1 Q. Schiermeier, J. Tollefson, T. Scully, A. Witze and O. Morton, *Nature*, 2008, **454**, 816–823.
2 B. O'Regan and M. Grätzel, *Nature*, 1991, **353**, 737–740.
3 A. Hagfeldt, G. Boschloo, L. Sun, L. Kloo and H. Pettersson, *Chem. Rev.*, 2010, **110**, 6595–6663.
4 A. B. Muñoz-García, I. Benesperi, G. Boschloo, J. J. Concepcion, J. H. Delcamp, E. A. Gibson, G. J. Meyer, M. Pavone, H. Pettersson, A. Hagfeldt and M. Freitag, *Chem. Soc. Rev.*, 2021, **50**, 12450–12550.
5 A. Sen, M. H. Putra, A. K. Biswas, A. K. Behera and A. Groβ, *Dyes Pigm.*, 2023, **213**, 111087.
6 C. E. Housecroft and E. C. Constable, *Chem. Sci.*, 2022, **13**, 1225–1262.
7 K. Prajapat, M. Dhonde, K. Sahu, P. Bhojane, V. Murty and P. M. Shirage, *J. Photochem. Photobiol., C*, 2023, 100586.
8 Y. Liu, T. Harlang, S. E. Canton, P. Chábera, K. Suárez-Alcántara, A. Fleckhaus, D. A. Vithanage, E. Göransson, A. Corani, R. Lomoth, V. Sundström and K. Wärnmark, *Chem. Commun.*, 2013, **49**, 6412–6414.
9 Y. Liu, P. Persson, V. Sundström and K. Wärnmark, *Acc. Chem. Res.*, 2016, **49**, 1477–1485.
10 S. Kaufhold and K. Wärnmark, *Catalysts*, 2020, **10**, 132.
11 L. Lindh, P. Chábera, N. W. Rosemann, J. Uhlig, K. Wärnmark, A. Yartsev, V. Sundström and P. Persson, *Catalysts*, 2020, **10**, 315.
12 T. Duchanois, L. Liu, M. Pastore, A. Monari, C. Cebrián, Y. Trolez, M. Darari, K. Magra, A. Francés-Monerris, E. Domenichini, M. Beley, X. Assfeld, S. Haacke and P. C. Gros, *Inorganics*, 2018, **6**, 63.
13 Y. Liu and K. Wärnmark, in *Emerging Photovoltaic Technologies : Photophysics and Devices*, ed. C. S. Ponseca, Jenny Stanford Publishing, Singapore, 2020, ch. 5, p. 374.
14 M. Pastore, S. Caramori and P. C. Gros, *Acc. Chem. Res.*, 2024, **57**, 439–449.
15 T. Duchanois, T. Etienne, C. Cebrián, L. Liu, A. Monari, M. Beley, X. Assfeld, S. Haacke and P. C. Gros, *Eur. J. Inorg. Chem.*, 2015, **2015**, 2469–2477.
16 T. C. B. Harlang, Y. Liu, O. Gordivska, L. A. Fredin, C. S. Ponseca, P. Huang, P. Chábera, K. S. Kjaer, H. Mateos, J. Uhlig, R. Lomoth, R. Wallenberg, S. Styring, P. Persson, V. Sundström and K. Wärnmark, *Nat. Chem.*, 2015, **7**, 883–889.
17 A. R. Marri, E. Marchini, V. D. Cabanes, R. Argazzi, M. Pastore, S. Caramori and P. C. Gros, *J. Mater. Chem. A*, 2021, **9**, 3540–3554.
18 A. R. Marri, E. Marchini, V. D. Cabanes, R. Argazzi, M. Pastore, S. Caramori, C. A. Bignozzi and P. C. Gros, *Chem.–Eur. J.*, 2021, **27**, 16260–16269.
19 L. Lindh, O. Gordivska, S. Persson, H. Michaels, H. Fan, P. Chábera, N. W. Rosemann, A. K. Gupta, I. Benesperi, J. Uhlig, O. Prakash, E. Sheibani, K. S. Kjaer, G. Boschloo, A. Yartsev, M. Freitag, R. Lomoth, P. Persson and K. Wärnmark, *Chem. Sci.*, 2021, **12**, 16035–16053.
20 M. Karpacheva, C. E. Housecroft and E. C. Constable, *Beilstein J. Nanotechnol.*, 2018, **9**, 3069–3078.
21 M. Karpacheva, V. Wyss, C. E. Housecroft and E. C. Constable, *Materials*, 2019, **12**, 4181.
22 E. Marchini, M. Darari, L. Lazzarin, R. Boaretto, R. Argazzi, C. A. Bignozzi, P. C. Gros and S. Caramori, *Chem. Commun.*, 2020, **56**, 543–546.
23 A. Reddy-Marri, E. Marchini, V. D. Cabanes, R. Argazzi, M. Pastore, S. Caramori and P. C. Gros, *Chem. Sci.*, 2023, **14**, 4288–4301.
24 M. Pastore, T. Duchanois, L. Liu, A. Monari, X. Assfeld, S. Haacke and P. C. Gros, *Phys. Chem. Chem. Phys.*, 2016, **18**, 28069–28081.
25 L. Liu, T. Duchanois, T. Etienne, A. Monari, M. Beley, X. Assfeld, S. Haacke and P. C. Gros, *Phys. Chem. Chem. Phys.*, 2016, **18**, 12550–12556.
26 S. Sarker, H. W. Seo, Y.-K. Jin, K.-S. Lee, M. Lee and D. M. Kim, *Electrochim. Acta*, 2015, **182**, 493–499.
27 H. Elbohy, H. El-Mahalawy, N. A. El-Ghamaz and H. Zidan, *Electrochim. Acta*, 2019, **319**, 110–117.